J|A|C|S
ARTICLES
Published on Web 05/17/2006

Chemically Controlled Self-Assembly of Protein Nanorings

Jonathan C. T. Carlson,[†] Sidhartha S. Jena,[§] Michelle Flenniken,[⊥] Tsui-fen Chou,[†] Ronald A. Siegel,[§,||] and Carston R. Wagner*[,†,‡]

Contribution from the Departments of Medicinal Chemistry, Chemistry, Pharmaceutics, and Biomedical Engineering, College of Pharmacy, University of Minnesota, Minneapolis, Minnesota 55455, and Center for Bio-Inspired Nanomaterials, Montana State University, Bozeman, Montana 59717

Received February 4, 2006; E-mail: wagne003@tc.umn.edu

Abstract: The exploitation of biological macromolecules, such as nucleic acids, for the fabrication of advanced materials is a promising area of research. Although a greater variety of structural and functional uses can be envisioned for protein-based materials, systematic approaches for their construction have yet to emerge. Consistent with theoretical models of polymer macrocyclization, we have demonstrated that, in the presence of dimeric methotrexate (bisMTX), wild-type *Escherichia coli* dihydrofolate reductase (DHFR) molecules tethered together by a flexible peptide linker ($ecDHFR_2$) are capable of spontaneously forming highly stable cyclic structures with diameters ranging from 8 to 20 nm. The nanoring size is dependent on the length and composition of the peptide linker, on the affinity and conformational state of the dimerizer, and on induced protein−protein interactions. Delineation of these and other rules for the control of protein oligomer assembly by chemical induction provides an avenue to the future design of protein-based materials and nanostructures.

Introduction

The engineering of synthetic nanostructures for biomedical or bioelectronic applications is likely to require the use of multiple building materials, just as living systems rely on nucleic acids for information content and proteins for chemical and functional diversity. As such, it is critical to advance the science of self-assembly in multiple biochemical realms. To date, only DNA has seen extensive use as a building material for studies of self-assembly, selected for the well-understood and robust structural specificity of sequence recognition.[1,2] DNA sequences that form two-dimensional arrays,[3] a three-dimensional octahedron,[4] and even enzyme-like structures[5,6] have been described. Recently, the greater richness of RNA secondary structure has been exploited to create intricately patterned nano-building blocks.[7]

Nucleic acids, however, play a secondary role in biological nanomaterials. Following nature's lead, several early efforts to design self-assembling protein architectures have been described. To date, these synthetic protein assemblies have chiefly recapitulated biological assembly mechanisms, forming filaments from self-complementary β-strands, coiled coils, or helix bundles,[8] or symmetric nanostructures assembled from naturally multimeric proteins.[9]

We noted that the intrinsic ligand-binding ability of many proteins offers another means to direct nanostructure assembly. Just as DNA sequence recognition and protein−protein interactions have evolved to pick one target out of a complex background, so too have drug molecules been designed to target one protein among many. We chose to explore the construction of reversible proteinaceous nanostructures as an extension of earlier work with chemical inducers of protein dimerization (CIDs),[10] bivalent drug molecules that simultaneously bind and connect two proteins. As illustrated in Figure 1A, by assembling a bivalent (or multivalent) protein and a bivalent ligand, protein−drug recognition creates a selective structural linkage and can produce cyclic or linear structures (vide infra). Demonstrations of this principle in the literature have been few. In one report, naturally tetrameric lectins were combined with synthetic bivalent disaccharides to reversibly assemble proteinaceous crystals.[11] Recently, streptavidin−biotin binding has been exploited to assemble two-dimensional lattices and specific cruciform nanostructures,[12] and to form internal cross-links in the active, kinesin-mediated assembly of tubulin into "nanow-

[†] Department of Medicinal Chemistry, University of Minnesota.
[‡] Department of Chemistry, University of Minnesota.
[§] Department of Pharmaceutics, University of Minnesota.
[||] Department of Biomedical Engineering, University of Minnesota.
[⊥] Montana State University.

(1) Seeman, N. C. *Trends Biotechnol.* **1999**, *17*, 437−443.
(2) Seeman, N. C. *Chem. Biol.* **2003**, *10*, 1151−1159.
(3) Li, X.; Yang, X.; Qi, J.; Seeman, N. C. *J. Am. Chem. Soc.* **1996**, *118*, 6131−6140.
(4) Shih, W. M.; Quispe, J. D.; Joyce, G. F. *Nature* **2004**, *427*, 618−621.
(5) Liao, S.; Seeman, N. C. *Science* **2004**, *306*, 2072−2074.
(6) Shen, W.; Bruist, M. F.; Goodman, S. D.; Seeman, N. C. *Angew. Chem., Int. Ed.* **2004**, *43*, 4750−4752.
(7) Chworos, A.; Severcan, I.; Koyfman, A. Y.; Weinkam, P.; Oroudjev, E.; Hansma, H. G.; Jaeger, L. *Science* **2004**, *306*, 2068−2072.
(8) Yeates, T. O.; Padilla, J. E. *Curr. Opin. Struct. Biol.* **2002**, *12*, 464−470.
(9) Padilla, J. E.; Colovos, C.; Yeates, T. O. *Proc. Natl. Acad. Sci. U.S.A.* **2001**, *98*, 2217−2221.
(10) Carlson, J. C. T.; Kanter, A.; Thuduppathy, G. R.; Cody, V.; Pineda, P. E.; McIvor, R. S.; Wagner, C. R. *J. Am. Chem. Soc.* **2003**, *125*, 1501−1507.
(11) Dotan, N.; Arad, D.; Frolow, F.; Freeman, A. *Angew. Chem., Int. Ed.* **1999**, *38*, 2363−2366.
(12) Ringler, P.; Schulz, G. E. *Science* **2003**, *302*, 106−109.

10.1021/ja060631e CCC: $33.50

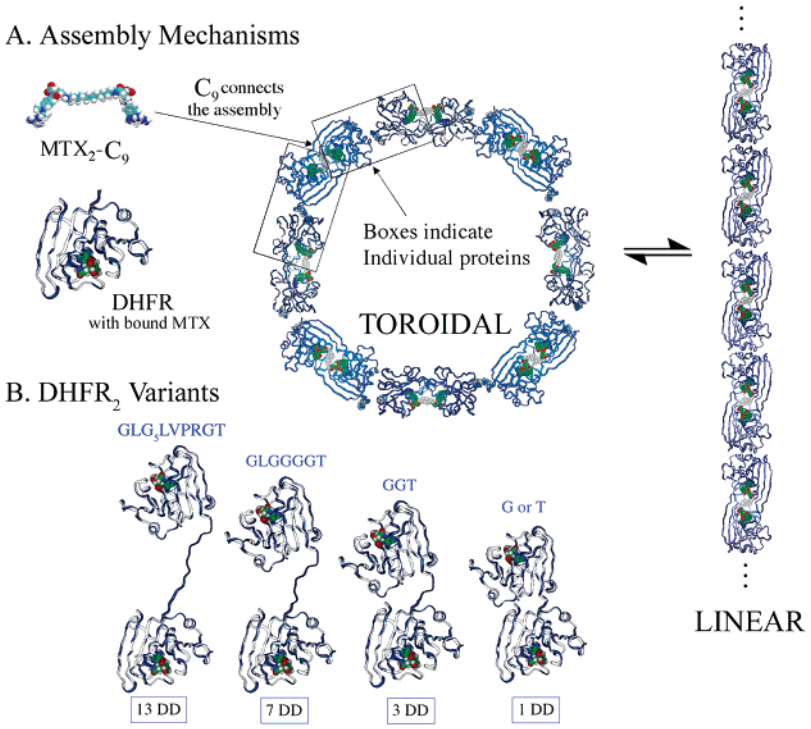

Figure 1. Assembly of ecDHFR$_2$ and MTX$_2$−C$_9$. (A) The individual components and proposed assembly mechanisms of the bisMTX and DHFR$_2$ system are diagrammed below. The conformational flexibility of the growing chain and thermodynamics of its connections will regulate the balance between cyclic and linear oligomers of 1DD-G and MTX$_2$−C$_9$. (B) Beginning with the 13DD plasmid (GLG$_5$LVPRGT), the DNA encoding the inter-DHFR linker was successively truncated by QuikChange mutagenesis to yield 7DD (GLG$_4$T), 3DD (GGT), 1DDG (G), and 1DDT (T). The images provide a graphical comparison of the relative linker proportions.

ires" and "nanospools".[13] The adaptation of protein nanostructures into useful tools will require further advances in the preparation of homogeneous components, as existing methods have not fully addressed the challenges of both polydispersity and incomplete assembly. Additionally, there is broad interest in methods capable of reliable patterning materials on the 5−50 nm scale, a size regime inaccessible to current techniques.[14]

Small molecule-induced assembly of protein supramolecular complexes is dependent on the induction of stabilizing protein−protein interactions by a tight binding bivalent ligand capable of inducing persistent and durable monomer connectivity over a wide range of ligand concentrations.[10] The methotrexate−dihydrofolate reductase CID system investigated by our laboratory fulfills these characteristics: bivalent methotrexate (bisMTX) derivatives bind to dihydrofolate reductase (DHFR) with picomolar affinity, forming robust complexes stabilized by protein−protein interactions.[10] Importantly, the ability of the free bisMTX ligands to adopt a stable folded conformation in solution significantly reduces the ligand-concentration dependence of induced protein assembly, a mechanism thoroughly characterized in our earlier work.[10] We therefore designed a set of DHFR fusion proteins with varying inter-domain linker lengths (Figure 1B) and characterized their bisMTX-mediated self-assembly into proteinaceous nanostructures.

Results and Discussion

To characterize the assembly of DHFR$_2$−bisMTX oligomers, mixtures of 10 μM 1DD-G, the shortest and simplest of the DHFR$_2$ fusion proteins, and MTX$_2$−C$_9$, a 9-methylene linked bisMTX dimerizer, were analyzed by gel filtration chromatography on a Superdex G200 column (GE Biosciences). As the relative ratio of MTX$_2$−C$_9$ was increased from 0.25 to 1.0 equiv, the peak corresponding to monomeric 1DD-G completely disappeared, with concurrent formation of a range of larger species (Figure 2A). At stoichiometries approaching or exceeding 1.0 equiv of MTX$_2$−C$_9$ (also abbreviated C$_9$), the smaller aggregates also disappeared, and assemblies of 1DD-G and MTX$_2$−C$_9$ were observed to elute in a broad peak centered at 20 min. This peak elution time corresponded to a calibrated Stokes radius (R_s) of 8.3 nm, substantially increased from the value of 3 nm observed for the monomer. The 1DD-G:C$_9$ aggregates proved to be remarkably stable. Kept in amber vials at room temperature, samples of assembled 1DD-G repeatedly analyzed by gel filtration over the course of 1 month showed no change in the observed size distribution.[15] The 1DD-G:C$_9$ aggregates also survived extreme dilution, remaining intact in transit through the gel filtration column at 50 nM total-protein concentration (the limit of detection in the gel filtration assay).

Encouraged by the formation of apparently robust assemblies, we pursued a theoretically rigorous characterization. The thermodynamics governing this mode of self-assembly have been investigated in the discipline of polymer chemistry, with particular attention given to ring-chain equilibria,[16−18] and in

(13) Hess, H.; Clemmens, J.; Brunner, C.; Doot, R.; Luna, S.; Ernst, K. H.; Vogel, V. *Nano Lett.* **2005**, *5*, 629−633.
(14) Whitesides, G. M.; Grzybowski, B. *Science* **2002**, *295*, 2418−2421.
(15) This is consistent with the exceptional stability of ecDHFR in aqueous solution. At 37 °C in pH 7 buffer, the catalytic activity of DHFR is lost with a half-life of approximately 1 month (data not shown).
(16) Jacobson, H.; Stockmayer, W. H. *J. Chem. Phys.* **1950**, *18*, 1600−1606.
(17) Ercolani, G.; Mandolini, L.; Mencarelli, P.; Roelens, S. *J. Am. Chem. Soc.* **1993**, *115*, 3901−3908.
(18) Ercolani, G. *J. Phys. Chem. B* **1998**, *102*, 5699−5703.

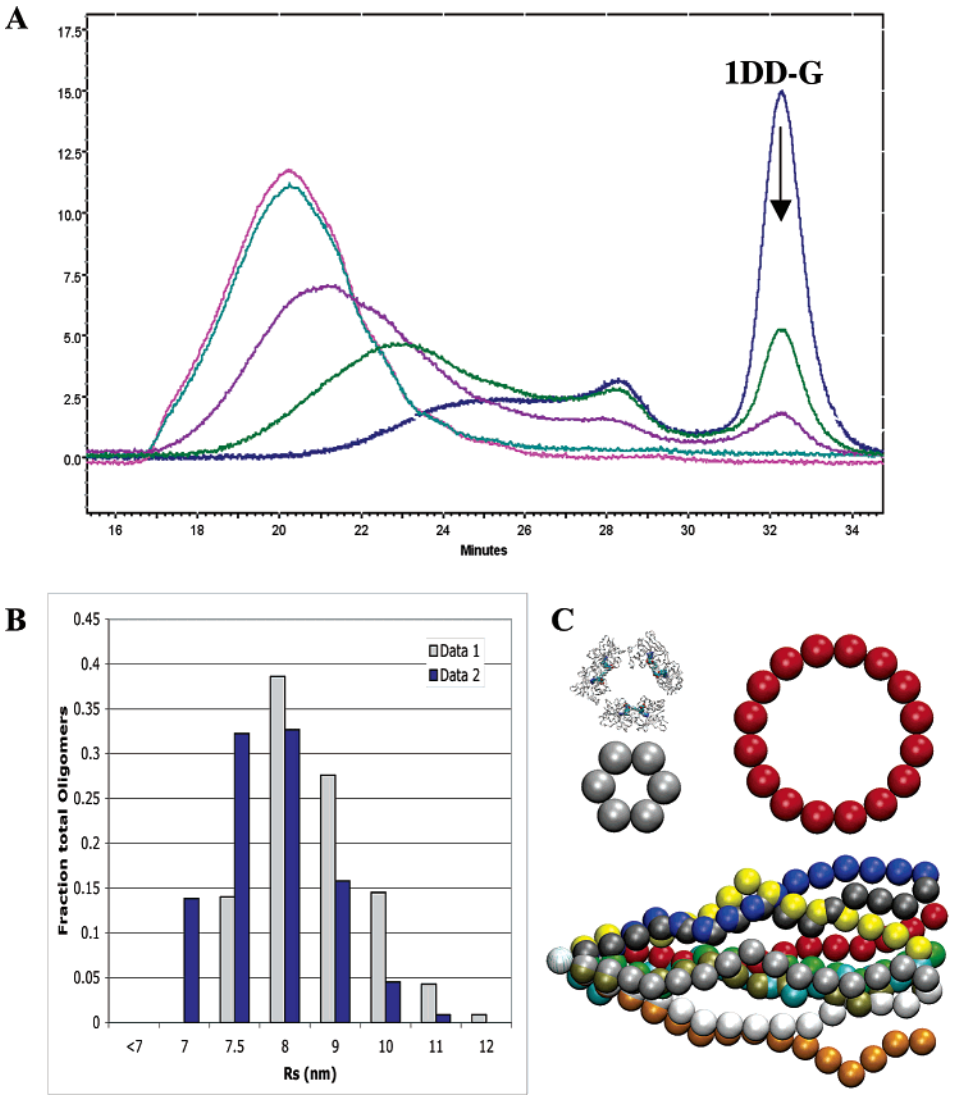

Figure 2. Assembly of 1DD-G and MTX_2-C_9. (A) Gel filtration profiles for 1DDG with 0.25, 0.5, 0.75, 1.0, and 1.25 equiv of added MTX_2-C_9 overlaid. Data were collected in sequential runs, beginning with the 1.25X sample, 30 min after initial mixing. The disappearance of the monomer peak near 32 min (dark blue) as the concentration of dimerizer increases is indicated by an arrow. (B) Nonnegative least-squares fit DLS data for the 1DD-G:C9 mixture at 12 μM in P500 buffer. The calculated best-fit distributions of particle sizes for two independent data acquisitions on the same sample are plotted. The weighted averages of these two distributions yield an average particle size for the mixture, $R_s = 8.3$ nm. (C) Toroidal conformations for potential aggregates, with coordinates derived from regular polygon geometry, with overlay of 10 random conformations for the octameric linear chain evaluated in HYDRO.

immunology, where the assembly of antibody−antigen complexes has been considered in detail.[19] In all polymerization systems with suitable end-to-end connectivity, the growing polymer chain has the option to react with an uncoupled partner in solution and extend linearly, or with its own tail, terminating chain growth and forming a ring.[20,21] The seminal work of Jacobsen and Stockmayer in the 1950s revealed that until the system reaches a critical concentration, only rings will be formed.[16] At low monomer concentrations, ring formation is highly favored, because the intramolecular effective molarity is much higher than the solution concentration. Synthetic chemists have demonstrated these effects in small-molecule systems that rely on metal ion coordination or hydrogen bonding.[20,22] Ercolani and co-workers have produced the most detailed theoretical description of ring formation, modeling the process in terms of the effective molarity (EM_n) for each of the cyclic species and the association constant for connection of the subunits.[17,18] Their model quantitates the significant degree to which ring formation is enhanced at low concentration and demonstrates that the propensity for ring formation increases in parallel with the association constant for the intermolecular connection. The extremely high affinity of DHFR−MTX binding, in tandem with micromolar protein concentrations, thus provides a strong driving force for ring formation. Ring size, in turn, is limited by entropic effects that strongly favor smaller oligomers. Introduction of conformational bias into the system can increase the EM of an individual oligomer, such as would be desired for the engineering of homogeneous self-assembled structures. Collectively, this theoretical framework strongly implies a cyclic conformation for the observed 1DD-G:C_9 aggregates.

(19) Perelson, A. S.; DeLisi, C. *Math. Biosci.* **1980**, *48*, 71−110.
(20) ten Cate, A. T.; Sijbesma, R. P. *Macromol. Rapid Commun.* **2002**, *23*, 1094−1112.
(21) Kricheldorf, H. R.; Rabenstein, M.; Maskos, M.; Schmidt, M. *Macromolecules* **2001**, *34*, 713−722.
(22) Vermonden, T.; van der Gucht, J.; de Waard, P.; Fleer, G. J.; Cohen Stuart, M. A. *Macromolecules* **2003**, *36*, 7035−7044.

Static and dynamic light-scattering experiments were therefore carried out to evaluate the mass, dimensions, and solution geometry of these nanoparticles. The utility of light scattering in characterizing particle shape is well known, as the critical hydrodynamic parameters of Stokes radius and radius of gyration (R_g) provide two unique variables to robustly distinguish between oligomers of alternate shape.[23,24] The ratio of the two parameters (R_g/R_s) yields a consistent descriptor of particle shape that is independent of absolute size: linear objects will have the highest R_g/R_s ratio and solid spherical ones the lowest, with other conformations falling at known discrete points on the spectrum between.

Dynamic light-scattering (DLS) data were collected at 90° to assess the Stokes radius of the 1DD-G:C_9 assemblies at their peak size (1 equiv of added C_9). For 12 μM 1DD-G:C_9, the DLS results indicated a distribution of hydrodynamic diameters from 14 to 22 nm, corresponding to an average Stokes radius of 8.3 nm (range: 7.98−8.66 nm), consistent with radii derived from the calibrated gel filtration data (Figure 2B). For static light-scattering (SLS) experiments, six samples were prepared, extending from 5 to 40 μM (0.17−1.41 mg/mL) total protein concentration. The scattering intensities were measured at regular intervals from 30° to 130°, and analyzed by the Zimm plot method,[25] yielding an average molecular weight of 240 ± 12 kD, with a radius of gyration of 10.8 ± 1 nm. This led to two conclusions: first, the molecular weight, 6.7-fold greater than that of 1DD-G, implied an average assembly containing seven 1DD-G subunits. Second, the SLS data indicate that the 1DD-G:C_9 assemblies must adopt a shape with an average R_g/R_s ratio of 1.3 ± 0.1.

To interpret these shape parameters, the program HYDRO was used to calculate the hydrodynamic properties for models of linear and toroidal 1DD-G:C_9 assemblies.[26] Toroidal structures with 3−9 subunits were generated, with the protein complexes approximated as rigid arrays of solid spheres (Figure 2C).[27] The calculated R_g/R_s ratios from HYDRO range from 1.17 to 1.29 for hexameric−nonameric toroids (Table 1A), in excellent general agreement with the experimental value of 1.27 derived from the light-scattering data. To contrast the cyclic and linear geometries, the octamer was chosen as a test case for further HYDRO calculations, and a set of 20 linear chains in random conformations was generated (Figure 2C). Parameters governing the flexibility of the chain were derived from Charmm simulations of the DHFR dimer and 1DDG conformational variability (data not shown). The calculated hydrodynamic data are summarized in Table 1B. While the mean R_s value for the linear conformer is very similar to that of a toroid, the linear-chain R_g value is significantly higher (16.5 vs 11.2 nm), yielding an R_g/R_s ratio of 1.75 ± 0.04, significantly different from the experimental value of 1.3 ± 0.1. Taken together, the calculated R_g/R_s ratios and experimental data strongly support a toroidal conformation for the 1DD-G:C_9 nanostructures.

Table 1. HYDRO Modeling Data for Toroidal and Linear Assemblies: (A) Calculated Hydrodynamic Dimensions of Circular DHFR−C_9 Toroids Ranging in Size from $n = 3$ to $n = 9$ and (B) Calculated Properties of the Linear Octamer Compared to the Calculated Octameric and Heptameric Toroids, and to the Experimental Data[a]

(A) Hydrodynamic Dimensions of DHRR–C_9 Toroids

n	R_s	R_g	R_g/R_s	longest axis (nm)	R_s exp (GelF)
9	9.72	12.49	1.28	29.1	
8	8.9	11.15	1.25	26.34	8.25
7	8.06	9.8	1.22	23.6	7.26
6	7.215	8.47	1.17	20.9	6.74
5	6.35	7.15	1.13	18.22	6.08
4	5.47	5.86	1.07	15.5	5.32
3	4.58	4.61	1.01	12.9	4.63

(B) Properties of Linear Octamer and Octameric and Heptameric Toroids

conformation	R_s	R_g	R_g/R_s ratio
linear octamer	9.45 ± 0.1	16.5 ± 0.5	1.75 ± 0.04
toroidal heptamer	8.1	9.8	1.22
toroidal octamer	8.9	11.15	1.25
experimental	8.3 ± 0.3	10.8 ± 1	1.3 ± 0.1

[a] The R_g/R_s ratio strongly supports a toroidal conformation.

The circular nature of these complexes was directly confirmed when the 1DD-G:C_9 assemblies were examined by negatively stained TEM (Figure 3). The structures observed are remarkably homogeneous, with no apparent linear fragments, fractured, or displaced toroids present; approximately 80% of the rings are geometrically circular, with minimal ellipticity seen in the remaining 20% (Figure 3A). The visibility of the toroids is enhanced by apparent pooling of the uranyl acetate contrast reagent in the center of the rings. At extreme magnification, the close correspondence of the nanoring proportions to those expected for a DHFR-derived toroid is evident (Figure 3B). These results provide another striking demonstration of the stability of the 1DD-G:C_9 nanorings, which remain intact through the staining and imaging process (2% uranyl acetate stain, pH 4) and subsequent air-drying.

Analysis of several wide-field images reveals that the observed toroids range from 20 to 28 nm in outer diameter (Figure 4A). The measurement process is illustrated for a cluster of nanorings in Figure 4B; in repeat trials, the error of the graphical sizing method was approximately 5%. By applying the HYDRO calculation of maximal toroid dimensions (Table 1) as a rough criterion, we sorted the distribution into four clusters, corresponding to oligomers of 6−9 subunits. The calculated longest axis was applied as the upper limit for each integer particle size; the resulting histogram of observed 1DD-G:C_9 oligomers appears in Figure 4C. This distribution is appealingly consistent with the SLS data, which also suggested an average 7-subunit assembly.

Armed with this careful characterization, we return to the structural analysis of the remaining $DHFR_2$ variants (Figure 1B), buttressed by the strong theoretical and mechanistic implication that these proteins will also form toroids. As the inter-DHFR linker is lengthened from a single amino acid to 3, 7, or 13 residues, the conformational flexibility of the $DHFR_2$ dimer increases, and the effective molarity of smaller oligomers is expected to increase in parallel. In tandem, entropic forces will drive the formation of smaller toroids. This led us to predict that the nanoring size-distribution could be tuned by adjusting

(23) Witz, J.; Timasheff, S. N.; Luzzati, V. *J. Am. Chem. Soc.* **1964**, *86*, 168−173.
(24) Townend, R.; Timasheff, S. N. *J Am. Chem. Soc.* **1960**, *82*, 3168−3174.
(25) Zimm, B. *J. Chem. Phys.* **1948**, *16*, 1099−1116.
(26) Garcia de la Torre, J.; Navarro, S.; Lopez Martinez, M. C.; Diaz, F. G.; Lopez Cascales, J. *Biophys. J.* **1994**, *67*, 530−531.
(27) Because of the simple geometric method used to generate coordinates for these structures, only coplanar conformations were considered. While the instantaneous conformation of a DHFR2 oligomer is unlikely to match one of these perfectly uniform structures, we hypothesized that they represent reasonable average conformations.

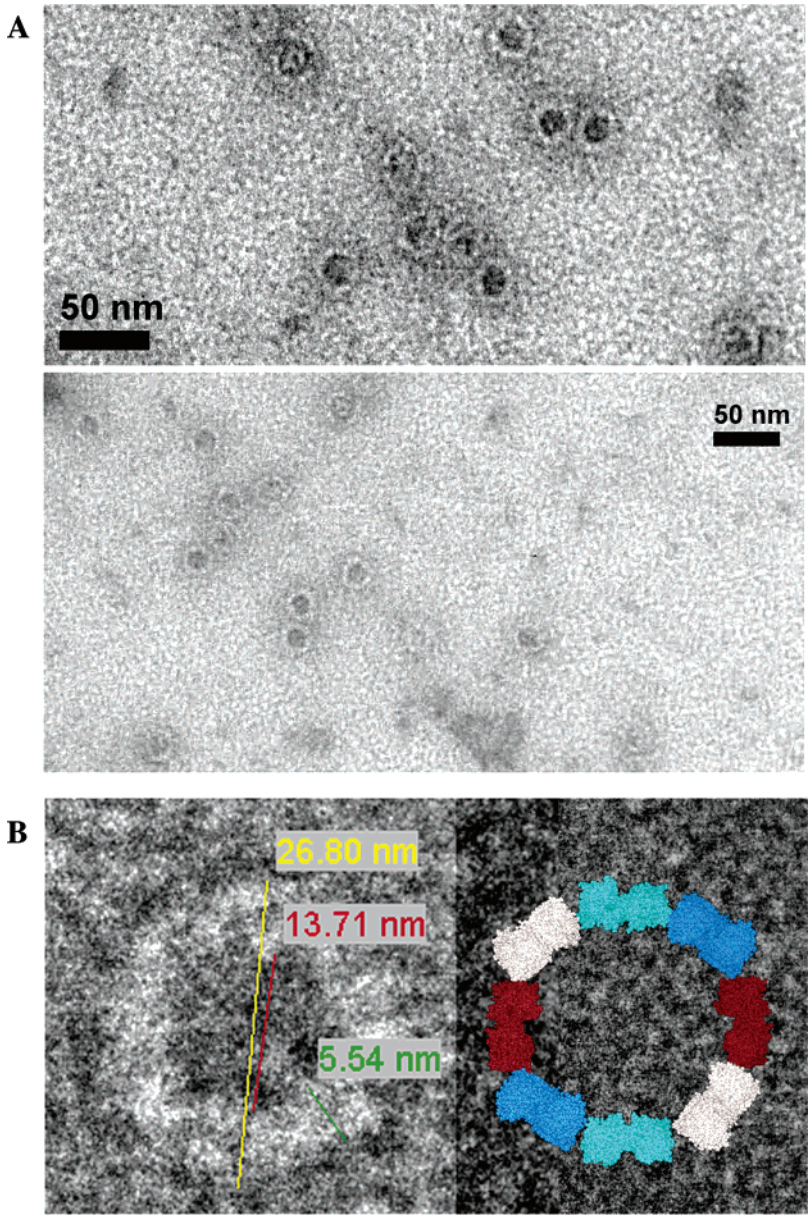

Figure 3. TEM imaging of 1DD-G:C9. Uranyl acetate stained images of 1DD-G:C9 deposited on a carbon grid. (A) Representative fields at 20 000× magnification illustrate consistent size and appearance of nanorings. 50 nm scale bars indicate scaling of the images. (B) At left, a single nanoring viewed at 63 000× magnification; the dimensions of the toroid are indicated. On the right, a space-filling model of an octameric ring is scaled to match the size of the TEM image, illustrating the matching proportionality of the ring shape.

the inter-domain linker length, a mechanism appealingly dependent not on intricate structural engineering but rather on fundamental biophysical chemistry.

We collected full assembly profiles for each of the $DHFR_2$ variants with MTX_2-C_9 and found that the observed nanoring size was indeed strikingly dependent on the length of the inter-DHFR linker. In Figure 5A, the elution profiles for MTX_2-C_9-assembled 13DD, 7DD, 3DD, and 1DDG are overlaid. Starting with the monomer peak at 32.4 min, which is constant for all five proteins, a landscape of discrete peaks marches leftward, enabling enumeration of each oligomer, indicated in Figure 5A by superimposed integer assignments for each peak. Unlike the elution profile for 1DD-G:C_9, the oligomer distributions for 13DD:C_9, 7DD:C_9, and 3DD:C_9 are well resolved, a consequence of the selectivity curve of the Superdex G200 matrix, which has much higher resolving power at Stokes radii of 2−6 nm. SLS and DLS data collected for the 3DD:C_9 and 13DD:C_9 aggregates were consistent with the toroidal geometry implied by 1DD-G:C_9 data and HYDRO modeling (data not shown).

Whereas the longer 13DD forms principally dimers, with progressively smaller quantities of trimer, tetramer, and pentamer, the 7DD dimer forms a spectrum of toroids spanning dimers to heptamers. In contrast, when the linker is shortened to 3 amino acids, virtually all of the assemblies are tetrameric or larger, with a preponderance of tetrameric nanorings. In Figure 5B, the gel filtration profiles of 1DDG and 1DDT are compared. The role of a single amino acid change in tuning the obtained distribution of rings is clearly apparent. The 1DDG peak spans oligomers from $n = 6$ to $n > 9$ (with sizes greater than 8 unresolved) and includes just traces of pentameric and tetrameric aggregates. In contrast, although the distribution of larger-sized oligomers at the left edge of the peak is quite similar, 1DDT forms a significantly increased amount of

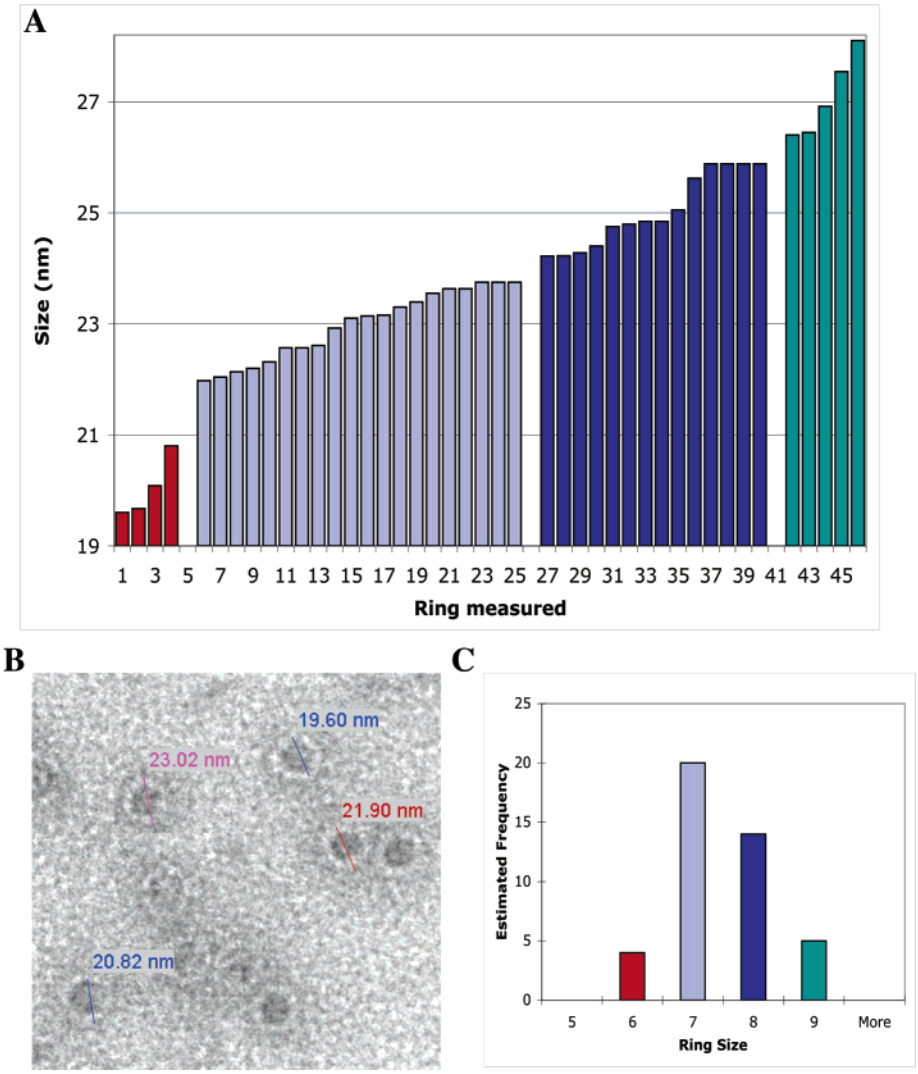

Figure 4. Distribution of 1DD-G:C_9 nanoring dimensions. (A) The diameters of 43 1DD-G:C_9 nanorings, measured from three TEM wide fields at 20 000× magnification, are graphed. The coloration corresponds to approximate oligomer size ranges derived from the HYDRO calculations; the "longest axis" measurement calculated for each toroid is used as an upper limit for that oligomer size. (B) The dimensions of four nanorings are measured in this image field, illustrating the method. (C) Histogram of ring sizes, based on the estimated size cutoffs applied to the data in part (A).

hexameric and pentameric rings. The responsiveness of oligomer size to a single amino acid substitution suggests a number of intriguing possibilities for future experiments.

Curious about the dynamic equilibrium of the observed oligomer distributions, we attempted to use gel filtration to purify a discrete subpopulation of nanorings. We chose to test 3DD because of the excellent resolution of the tetramer−hexamer peaks. Figure 5C illustrates the results of these fractionation stability experiments. A fully assembled 3DD−C_9 mixture was injected onto the G200 column, and the eluted material was collected in two fractions, one containing heptameric and larger assemblies, the other tetramers−hexamers. Reanalysis of these separate fractions via gel filtration revealed that the segregated oligomer populations retained their original sizes; the individual nanorings were stable to purification. Further testing demonstrated that both purified nanoring fractions remained stable in dilute solution at 4 °C for days (Figure S1).

Conclusions

Altogether, these experiments demonstrate the creation of exceptionally stable proteinaceous nanorings, resistant to both adverse environmental conditions and high dilution. The dimensions of these rings can be tuned by changing the length of the intramolecular protein linker, and individual size ranges of oligomers can be purified. When the rules for the design of ligand-induced dimerization systems[10] are combined with recent theoretical models of supramolecular assembly,[18,28] our results establish the underlying principles required for the design of stable self-assembling protein-based nanoarchitectures. Appealingly, the intrinsic conformational flexibility of the $DHFR_2$ building block allows equilibrium and kinetic factors to dictate nanoring geometry, resulting in preferred structures such as the stable tetramer observed for 3DD:C_9. Consistent with the theoretical framework outlined by Ercolani,[18,28] the size distribution of the assembled toroids depends on the subtle balance between entropy and conformational dynamics. The entropic factors that favor the smallest feasible oligomer are offset by the ring strain imposed by the intrinsic stiffness of the $DHFR_2$ building blocks, which dictates the EM of the individual toroids. A predictive method for analyzing the relationship between $DHFR_2$ conformation and assembly will be described separately

(28) Ercolani, G. *J. Phys. Chem. B* **2003**, *107*, 5052−5057.

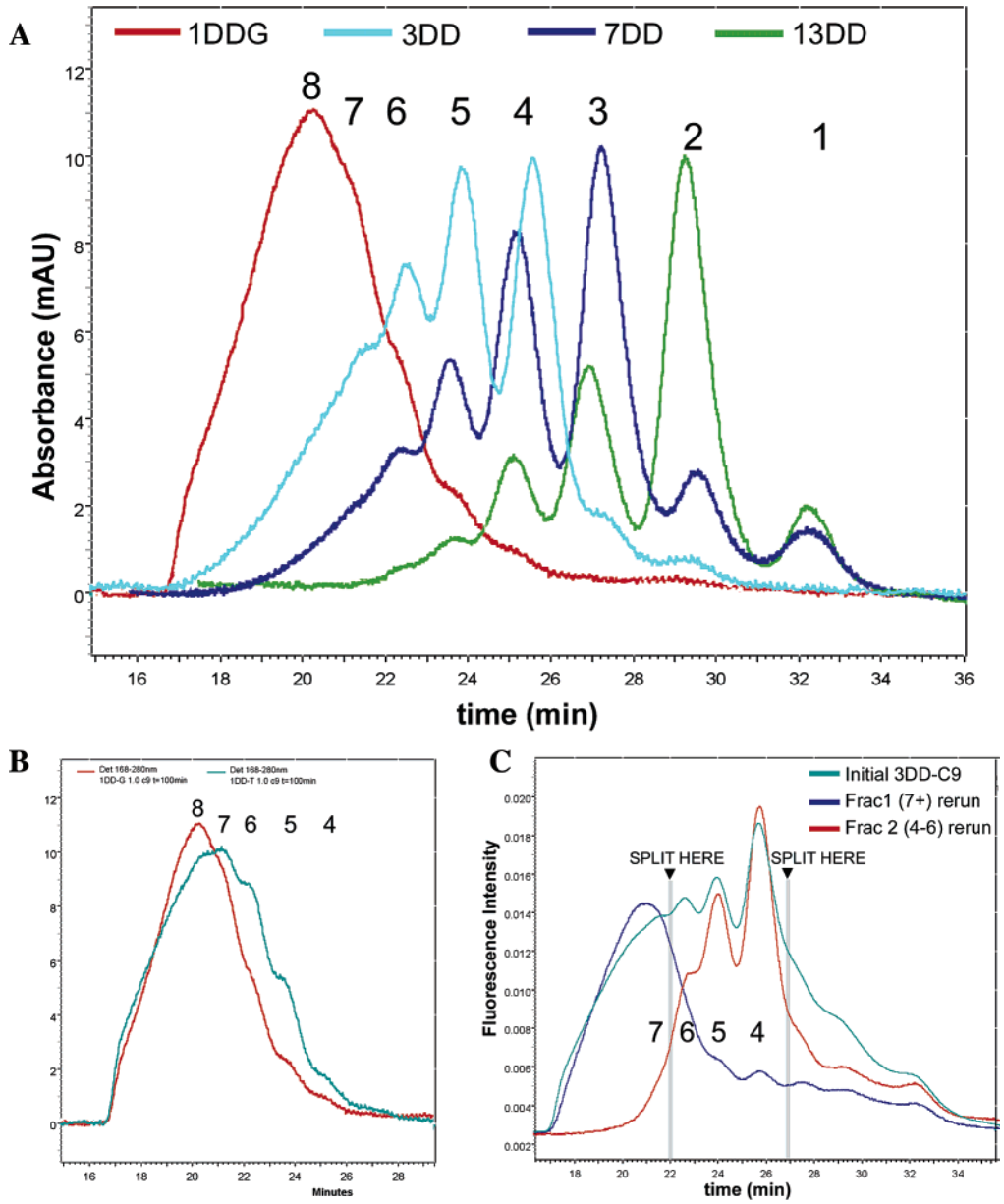

Figure 5. Regulation of oligomer size as a function of linker. (A) In the top panel, the gel filtration traces for fully assembled (1:1) 1DD-G:C_9, 3DD−C_9, 7DD−C_9, and 13DD−C_9 are overlaid, illustrating the ability to assign each peak to a discrete nanoring size, from dimer to octamer. (B) The overlaid traces for 1DD-G:C_9 (red) and 1DDT−C_9 (green) at bottom left illustrate the ability of a single amino acid substitution to tune the observed oligomer pattern. (C) The Superdex G200 elution profile of 40 μM 3DD−C_9 (1:1). The material from the start of the peak until the first split point was collected in one fraction, representing oligomers of $n \geq 7$. The complexes that eluted between the first and second split points ($n = 4-6$) were collected into a second fraction. When each of the collected fractions was reinjected onto the column, the segregated oligomer sizes remained stable.

(Carlson, J. C. T.; Wagner, C. R., manuscript in preparation). As the design of fusion proteins with controlled intramolecular orientations remains difficult, this robust biophysical mechanism is a potentially valuable tool.[8]

When compared to avidin−biotin, the workhorse pair of the protein self-assembly literature, the bisMTX−$DHFR_2$ construct may have several advantages. Unlike the members of the tetrameric 68 kDa avidin family, the 18 kDa ecDHFR is intrinsically a monomer, well suited for facile engineering of other fusion protein constructs. Indeed, in many cases, the rigid tetrameric nature of the avidins is an obstacle to nanostructure design and/or characterization. Although the extraordinarily tight binding affinity of biotin and streptavidin provides particularly robust structural connections, slightly lower binding affinities may provide improved error-correction for some self-assembly applications. Indeed, substantial research efforts have sought to engineer avidin derivatives to possess DHFR-like characteristics.[29]

Ultimately, the properties of the dimerizing ligand are also important in regulating the energetics and geometry of self-assembly. Although incompletely characterized thus far, the ability of the bisMTX dimerizers to adopt a folded conformation in solution[10] should promote stable assemblies by the same mechanisms operative for simple dimerization. In parallel with the effects of protein engineering, modifications in the dimerizer linker length will also alter the geometric characteristics regulating $DHFR_2$ nanoring formation (data not shown).

(29) Laitinen, O. H.; Nordlund, H. R.; Hytonen, V. P.; Uotila, S. T.; Marttila, A. T.; Savolainen, J.; Airenne, K. J.; Livnah, O.; Bayer, E. A.; Wilchek, M.; Kulomaa, M. S. *J. Biol. Chem.* **2003**, *278*, 4010−4014.

Refinement of this assembly mechanism as a route to synthetic bio-polymeric materials, in addition to discrete oligomers, is a focus of ongoing research. In principle, a proteinaceous or hybrid protein−organic polymer with noncovalent bisMTX linkages would represent a pharmaceutically reversible material. In the presence of excess concentrations of an appropriate competitive drug molecule, the connections stitching the polymer together could be specifically dissolved, particularly once an initial competitive binding event has reduced the macrocyclic oligomers to linear species. Many biomedical applications can be envisioned for the proposed drug-responsive material.

Finally, the set of $DHFR_2$ constructs is well suited for development of more elaborate self-assembling architectures in future studies. The N and C termini of the proteins, as discussed previously, are 180° removed from the dimer interface, permitting ready construction of trimeric and tetrameric fusion proteins. In this manner, assembly of $DHFR_2$ nanorings could create circular clusters of other structural or functional proteins, such as artificial antibodies or templates for nano-molecular gears. In addition, our ability to prepare protein polygons suggests a future pathway for the design and preparation of self-assembling protein polyhedra.[30] Future efforts to identify chemically oligomerizable proteins will allow the power of chemical genetics and protein structure database analysis to be employed for nanotechnology.

Materials and Methods

Protein Expression and Purification. The detailed procedure for construction of the $DHFR_2$ plasmids will be described in detail elsewhere. JM-105 *E. coli* containing the engineered $DHFR_2$ plasmid of interest were cultured in LB or TB broth containing ampicillin (100 ug/mL). Cultures were grown at 37 °C in 2 L flasks with stirring and aeration to an OD_{600} of 0.6−0.8, whereupon IPTG was added to a concentration of 0.35 mM. The cultures were returned to the shaker and incubated for another 4−6 h, at which point the OD_{600} was typically >1.5. Cells were harvested through centrifugation at 7500*g* for 30 min at 4 °C. Typically, 3−4 g of cell paste was obtained per liter of LB culture, and 5−6 g per liter of TB culture.

The cell paste (approximately 7 g) was suspended in 6−7 mL of lysis buffer plus lysozyme (10 mM KH_2PO_4, 0.1 mM EDTA, 1 mM DTT, pH 8, 1 mg/mL lysozyme) and incubated at room temperature with gentle shaking for 30 min. The partially lysed cells were then cooled in an ice bath and sonicated 12 × 30 s, with ≥2 min between each repetition to allow the lysate to cool to 4−6 °C. The slurry was centrifuged at 40 000*g* for 45 min at 4 °C. The supernatant was decanted and saved. Unlike the methods described for purification of monomeric DHFR, a second round of sonication was not performed; this maximized the protein concentration, important for the MTX-column loading step. Finely ground ammonium sulfate was added with vigorous magnetic stirring to the combined supernatants to reach 30% saturation over 75 min at 4 °C. The slurry was centrifuged at 40 000*g* for 25 min at 4 °C. The supernatant was dialyzed for 2 or more hours in 2 L of equilibration buffer (10 mM KH_2PO_4, 0.1 mM EDTA, 0.5 M KCl, 1 mM DTT, pH 6).

In the optimized method, the dialyzed protein solution was loaded (2 mL/min) at full concentration onto a methotrexate column that had been prepared with phosphate buffer (50 mM KH_2PO_4, 1 mM EDTA, 1 mM DTT, pH 6). Once the retentate was fully loaded, the column was washed with high salt buffer (50 mM KH_2PO_4, 1 mM EDTA, 1 mM DTT, 1 M KCl, pH 6) until A_{260} and A_{280} of the flow-through were less than 0.05. The partially purified protein was initially eluted with 200 mL of 1 mM folate buffer (10 mM KH_2PO_4, 0.1 mM EDTA, 1 M KCl, 1 mM folate, 1 mM DTT, pH 9) at 1 mL/min, collected in 8 mL fractions. The gradient program then increased the elution buffer to 15 mM folate over the next 100 min, and finished with a further 200 mL of 15 mM folate buffer. The eluted fractions were assayed for DHFR activity via the assay described below. The high-folate fractions with DHFR activity were held in reserve, and the low-folate fractions with activity were combined and dialyzed four times against 2 L of dialysis buffer (50 mM Tris, 1 M NaCl, 1 mM EDTA, 0.5 mM DTT, pH 8) for 4 h each to remove folate. One final dialysis against 2 L of DEAE column equilibration buffer (10 mM Tris, 1 mM EDTA, 1 mM DTT, pH 7.2) for 4 h in preparation for loading onto column was completed. The dialyzed retentate was then loaded onto a DEAE Cellulose column prepared with equilibration buffer (above) at 1.5 mL/min. The column was washed with 200 mL of the same equilibration buffer and then eluted in a 500-min linear gradient between equilibration buffer and DEAE elution buffer (10 mM Tris, 0.5 M KCl, 1 mM EDTA, 1 mM DTT, pH 7.2) with 8 mL fractions collected. Collected fractions were assayed for DHFR activity as previously described and analyzed for A_{280} and A_{260}.[31] Fractions containing pure $DHFR_2$ were combined and concentrated with a Millipore Amicon Ultrafiltration YM-3 Membrane to approximately 2 mg/mL. The purity of the protein and progress of the purification was assayed with 12% SDS-PAGE (Invitrogen) and gel filtration chromatography (see below).

Gel Filtration. Gel filtration samples were prepared in P500 buffer (0.5 M NaCl, 50 mM KH_2PO_4, 1 mM EDTA, pH 7.0) with 5% (v/v) glycerol. Samples were mixed in 200 μL vial inserts (Chromtech, MN), with the components added in a specific order to ensure reproducibility: first buffer, then $DHFR_2$, and then dimerizer. Samples were incubated at room temperature for a minimum of 20 min prior to analysis. The mixture was fractionated with a Superdex G200 size exclusion column (GE Biosciences), eluted with P500 buffer, and the relative peak sizes quantitated by absorbance at 280 nm. Samples were stored in amber vials and carefully shielded from direct light to avoid long-term MTX photodegradation. The Superdex G200 column was calibrated with a molecular weight standards kit (GE Biosciences). The test reagents were Blue Dextran (MW = 2×10^6), used to determine the void volume of the column, thyroglobulin (669 kDa), ferritin (440 kDa), catalase (232 kDa), aldolase (158 kDa), and bovine serum albumin (66 kD). To extend the calibration curve to the lower molecular weight range, $DHFR_2$-3DD (36.2 kD), DHFR (18.0 kDa), and cytochrome C (12.4 kDa) were also included. The calibration curves were calculated as recommended by the manufacturer. The linear molecular weight calibration plotted Log MW versus K_{av}, where $K_{av} = (V_E - V_o)/(V_t - V_E)$; V_E is the elution volume of the MW standard; V_o is the void volume (elution volume of blue dextran); and V_t is the total column volume (24 mL). The R^2 value for the line of best fit was 0.986. The Stokes radius calibration was determined by plotting $(-\log(K_{av}))^{0.5}$ versus Stokes radius, yielding a straight line with an R^2 of 0.994.

Sample Preparation for Light Scattering. All samples for light-scattering experiments were prepared by methods designed to maximally reduce dust contamination. Water used for cleaning the sample tubes was triple-filtered through a 0.2 μm PES membrane (Corning). The acetone used for rinsing and drying the sample tubes was filtered through a 0.2 μm nylon filter membrane (Chromtech, MN), then triple filtered through a 0.02 μm aluminum oxide membrane (Anopore, Whatman, UK). Sample tubes (10 × 100 mm) and plastic caps were initially cleaned by 5 min of sonication in a water bath (Fisher Scientific). All subsequent sample preparation was conducted inside a laminar flow tissue-culture hood to reduce ambient dust burden. The clean sample tubes and caps were rinsed thoroughly with 0.2 μm-filtered water, rinsed a minimum of two times with 0.02 μm-filtered acetone, and left open inside the hood until the acetone evaporated, when they were recapped.

(30) Ercolani, G. *J. Phys. Chem. B* **2003**, *107*, 5052−5057.

(31) Taira, K.; Benkovic, S. J. *J. Med. Chem.* **1988**, *31*, 129−137.

Stock solutions of $DHFR_2$ proteins were equilibrated with P500 buffer at pH 7 via dialysis or by serial concentration/dilution in an Amicon concentrator (Millipore, MA). The concentration of the protein solution was then determined spectrophotometrically; an extinction coefficient of 62 200 M^{-1} cm^{-1}, double the literature value for DHFR, was employed.[31] This raw concentration was corrected for the optical purity of protein (the fraction of the total A_{280} accounted for by the protein), as determined by gel filtration chromatography. MTX_2-C_9 stock solutions were prepared in DMSO and assayed spectrophotometrically to determine their concentration. An extinction coefficient of 47 400 M^{-1} cm^{-1} in pH 13 NaOH, double the value observed for a MTX γ-amide, was employed.[32] The stock concentration was calibrated so that the final samples contained less than 2% DMSO. The dimerizer solution was then diluted 1:2 or 1:3 into P500 buffer. The protein and dimerizer solutions, inside the tissue-culture hood, were each filtered three times with a 0.02 μm Anopore syringe filter (Whatman, UK).

Autoclaved micropipet tips, rinsed three times in 0.02 μm-filtered buffer immediately prior to use, were used in all subsequent sample preparations. Appropriate volumes of the $DHFR_2$ and MTX_2-C_9 stocks to yield a 1:1 stoichiometric mixture were combined and thoroughly yet gently mixed in a rigorously cleaned screw-top vial with a Teflon lid liner.

This mixture was incubated at room temperature for 15−20 min, whereupon aliquots were withdrawn, added to the clean sample tubes, and diluted in varying ratios with ultrafiltered P500 buffer to yield the experimental samples.

Laser Light Scattering. Light-scattering studies employed a custom-built apparatus with a variable-power 488 nm argon ion laser light source (Lexel Laser, Inc., CA) and a goniometer-photodetector system (Brookhaven Instrument Corp., NY). Laser power, adjusted as necessary to sample the range of concentrations and particle sizes, ranged from 50 to 200 mW. For the dynamic light-scattering (DLS) experiments, the autocorrelated data were analyzed by both cumulant and nonnegative least-squares (NNLS) regression analysis.[33,34] For the static light-scattering experiments, data were collected across a range of angles from 30° to 130°: 30°, 35°, 40°, 45°, 50°, 60°, 70°, 80°, 90°, 100°, 110°, 120°, and 130°. The instrument was calibrated with a toluene standard sample.

Hydrodynamic Calculations. For calculations made with HYDROPRO, a model of $DHFR_2$−1DDG was constructed in InsightII (Accelrys, CA) by rearranging and linking (N-term−C-term) the two DHFR subunits from the 4DFR crystal structure.[35] Calculations on monomeric DHFR used the B chain from the 4DFR dimer structure. HYDROPRO employs a two-stage bead-shell modeling process to calculate hydrodynamic properties of globular proteins on the basis of their atomic structure. In the first stage, a spherical bead of calibrated size replaces each heavy atom in a crystal structure. The space defined by these larger beads is used to create a hollow shell, composed of smaller spheres, that is successively refined to yield accurate hydrodynamic properties. Per the authors' recommendation, the atomic element size was set to 3.1 Å for construction of the initial bead model; for the extrapolated shell-model calculation, a bead-diameter range of 2.05−1.05 Å and sampling interval of 0.2 Å were employed.

HYDROPRO calculations on DHFR aggregates used bead radii of 2.15 and 2.0 nm. The coordinates for the toroidal structures were initially calculated trigonometrically in Microsoft Excel by deriving the geometric spacing for the appropriate regular polygon. To test the effect of bead size on calculated toroid parameters, a Fortran program was written to automatically generate the appropriate coordinates and HYDRO input file for the $n = 3$ to $n = 9$ toroids. A second Fortran program was written to derive coordinates and produce HYDRO input files for the randomly sampled linear chains. This code applied a simple algorithm to three-dimensionally randomize the intramolecular bend angle of each element of the virtual $DHFR_2$ chain. The randomization function was tuned to produce a range of outside bend angles from ~108° (matched to the vertex angle of a pentagon) to 180° (linear). The calculated R_s and R_g values of 20 structures generated by this means were tabulated for summary statistics. To verify the geometric accuracy of the computer-generated structures, the pseudo-PDB file generated by HYDRO was loaded into VMD for visual inspection.

Transmission Electron Microscopy. Samples of MTX_2-C_9 and 1DDG in P500 buffer were filtered by the methods described for the light-scattering experiments above, then mixed in 1:1 stoichiometry at 40 μM concentration. These samples were stored on ice and shipped to Montana for microscopy. The 1DD-G:C_9 oligomer solution was passed through a Superose 200 gel filtration column to reduce the salt concentration and the protein peak collected in one band. This material was concentrated by centrifugation and stored at 4 °C prior to TEM analysis.

The 1DD-G:C_9 oligomer mix was deposited on 300-mesh copper grids that had been sequentially Formvar and carbon coated. The grids were blotted and stained with 2% uranyl acetate by standard techniques, as described in ref 36.

In screening and annotating the wide field 1DD-G:C_9 TEM images, rare rings with more than 10% apparent ellipticity were excluded from the dimensional analysis. In cases where minor ellipticity was observed, the reported diameter is the average of the perpendicular long and short axes.

Acknowledgment. We would like to thank the Division of Medicinal Chemistry−American Chemical Society for a Predoctoral Fellowship to J.C.T.C. This research was supported by a Ziagen Faculty Development Grant (C.R.W.) from the University of Minnesota, Department of Medicinal Chemistry, and an AHC Seed-grant (C.R.W.) from the University of Minnesota Academic Health Center. We would also like to thank Dr. Trevor Douglas for access to the electron microscopy facilities at Montana State University.

Supporting Information Available: Reanalysis by gel filtration of purified nanoring fractions from Figure 5C after 41 h at 4 °C (Figure S1). This material is available free of charge via the Internet at http://pubs.acs.org.

JA060631E

(32) Rosowsky, A.; Forsch, R. A.; Freisheim, J. H.; Galivan, J.; Wick, M. J. *J. Med. Chem.* **1984**, *27*, 888−893.
(33) Morrison, I. D.; Grabowski, E. F.; Herb, C. A. *Langmuir* **1985**, *1*, 496−501.
(34) Koppel, D. E. *J. Chem. Phys.* **1972**, *57*, 4184−4820.
(35) Bolin, J. T.; Filman, D. J.; Matthews, D. A.; Hamlin, R. C.; Kraut, J. *J. Biol. Chem.* **1982**, *257*, 13650−13662.
(36) Flenniken, M. L.; Willits, D. A.; Brumfield, S.; Young, M. J.; Douglas, T. *Nano Lett.* **2003**, *3*, 1573−1576.